Energy transport in the presence of entanglement

A. A. Cifuentes and F. L. Semião
Centro de Ciências Naturais e Humanas, Universidade Federal do ABC, 09210-170 Santo André, São Paulo, Brazil
(Received 19 January 2017; published 2 June 2017)

In this work we investigate how the presence of initial entanglement affects energy transport in a network. The network has sites dedicated to the incoherent input or output of energy and intermediate control sites where initial entanglement can be established. For short times, we find that the initial entanglement in the control sites provides a robust efficiency enhancer for energy transport. For longer times, dephasing considerably damps the quantum correlations and the advantage of having initial entanglement tends to disappear in favor of the well-known mechanism of noise-assisted transport. Our findings from the study of these two mechanisms may be useful for a better understanding of the relation between nonclassicality and transport, a topic of potential interest for quantum technologies.

DOI: 10.1103/PhysRevA.95.062302

I. INTRODUCTION

Quantum control [1] and quantum transport (QT) [2] play a prominent role in modern applications of quantum dynamics. In particular, quantum networks (QNs) are extensively used to investigate the phenomenon of energy propagation and its relation to quantum coherence. Paradigmatic examples are that of light harvesting complexes [3–7] and nanodevices [8]. This kind of investigation led to the discovery of noise-assisted transport (NAT) [3,9], where the interaction with the environment helps to enhance transport efficiency when the system parameters are appropriately tuned. In the context of light harvesting complexes, there are investigations about the capability of the dynamics in promoting the manifestation of quantum correlations [10–12]. Unfortunately, complete control over system state preparation and its evolution is not yet possible in real photosynthetic systems, let alone the use of characterization tools from quantum information science.

A natural step is then to ask how especially arranged QNs of controlled quantum systems can be used to critically assess the role of quantum coherences and correlations in the phenomenon of energy transport [13,14]. In this work we are interested in this kind of investigation. In other words, we are interested in the active role of state preparations and external control over transport efficiency. These situate our work in the context of quantum technologies where, instead of having a naturally occurring network, such as a photosynthetic complex, one can deliberately engineer a system, prepare its states, and drive it to study its response. This is precisely the case of setups such as trapped ions and cavity or circuit quantum electrodynamic systems, just to name a few examples. In these systems, control is usually achieved by means of interaction with external fields. In particular, it has been recently shown that cleverly chosen external time-dependent drivings can assist quantum tunneling between nodes in a QN [15–17]. Here we employ this idea to engineer a QN suitable to our purpose of studying how quantum correlations actively influence energy transport.

This article is organized as follows. In Sec. II we present the network model used in this work. Our results are presented in Sec. III, where we carefully investigate the role of quantum correlations and environment in the efficiency of energy transport through the network. In Sec. IV we summarize our findings and present our final remarks.

II. MODEL

The basic two-dimensional network we are interested in is depicted in Fig. 1. For our purposes, it is important that interaction between sites 1 and 3 and between sites 2 and 4 are negligible. By doing that, we are able to study how energy injected in site 1 arrive at site 3 through indirect pathways $1 \leftrightarrow 2 \leftrightarrow 3$ and $1 \leftrightarrow 4 \leftrightarrow 3$. For the sake of generality though, we start from a scenario where each site couples to the rest of the network and, by adapting the driving mechanism in [15,16], we end up with the effective system depicted in Fig. 1.

The network Hamiltonian with external driving reads

$$\hat{\mathcal{H}}(t) = \hat{\mathcal{H}}_0(t) + \hat{\mathcal{H}}_c, \tag{1}$$

with the total on-site energies subjected to external driving described by $\hat{\mathcal{H}}_0(t) = \hbar \sum_{j=1}^{4} E_j(t)\hat{\sigma}_j^+\hat{\sigma}_j^-$, where

$$E_j(t) = \omega_j + \Delta\omega_j + \eta_{d,j}\omega_{d,j}\cos(\omega_{d,j}t + \phi_j), \tag{2}$$

and the coherent hopping given by

$$\hat{\mathcal{H}}_c = \hbar \sum_{jk=1;k>j}^{4} c_{jk}(\hat{\sigma}_j^+\hat{\sigma}_k^- + \hat{\sigma}_j^-\hat{\sigma}_k^+), \tag{3}$$

where

$$\Delta\omega_j = \Delta\omega(\Theta_1 j_1 + \Theta_2 j_2), \tag{4}$$

with Θ_1 and Θ_2 positive integers [18], $\hat{\sigma}_j^+$ and $\hat{\sigma}_j^-$ two-level raising and lowering operators at site j, respectively, $\eta_{d,j}$ and $\omega_{d,j}$ basically the amplitude and angular frequency of the driving field acting on site j, and c_{jk} the coherent transfer rate between sites j and k. Also, ϕ_j are site-dependent phases in the external time-dependent fields. Notice that we keep the possibility of having non-negligible couplings between any pair of sites. In Appendix A we show how a clever choice of the external driving field parameters effectively implements the scenario depicted in Fig. 1. In the next section, the simulations will be made supposing equal coupling strengths for all sites, i.e., $c_{jk} = c$, and using driving parameters that effectively turn off the couplings $1 \leftrightarrow 3$ and $2 \leftrightarrow 4$, which is the scenario

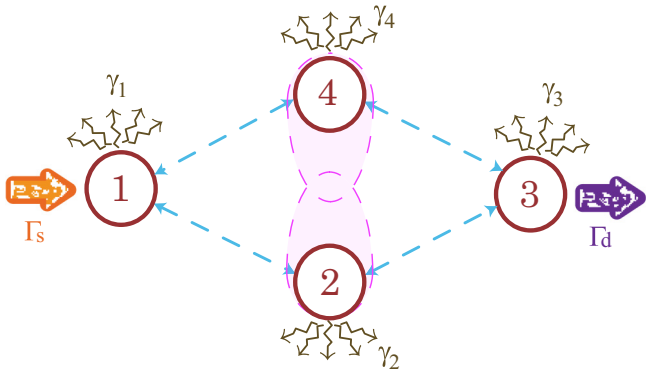

FIG. 1. Different dynamical elements of the effective network. Represented are the energy pump Γ_s at site 1, the energy drain Γ_d at site 3, the decoherence γ_k, and the effective energy hopping between sites (double-headed dashed arrows). Also, the possibility of having entangled states initially prepared for sites 2 and 4 is represented by the shadowed area delimited by a dashed contour.

considered in Fig. 1. Details are found in Appendices A and B.

The dynamics of the QN depicted in Fig. 1, which is our system of interest, is ruled by the master equation [19]

$$\frac{d\hat{\rho}}{dt} = -\frac{i}{\hbar}[\hat{\mathcal{H}}(t),\hat{\rho}] + \mathcal{L}_s(\hat{\rho}) + \mathcal{L}_d(\hat{\rho}) + \mathcal{L}_{\text{deph}}(\hat{\rho}), \tag{5}$$

where the source superoperator

$$\mathcal{L}_s(\hat{\rho}) = \Gamma_s(-\{\hat{\sigma}_1^-\hat{\sigma}_1^+,\hat{\rho}\} + 2\hat{\sigma}_1^+\hat{\rho}\hat{\sigma}_1^-) \tag{6}$$

accounts for the incoherent input of energy into the system through site 1 at a pump rate Γ_s, the drain superoperator

$$\mathcal{L}_d(\hat{\rho}) = \Gamma_d(-\{\hat{\sigma}_3^+\hat{\sigma}_3^-,\hat{\rho}\} + 2\hat{\sigma}_3^-\hat{\rho}\hat{\sigma}_3^+) \tag{7}$$

represents an incoherent loss of energy through site 3 at a rate Γ_d, and the dephasing superoperator

$$\mathcal{L}_{\text{deph}}(\hat{\rho}) = \sum_{k=1}^{N}\gamma_k(-\{\hat{\sigma}_k^+\hat{\sigma}_k^-,\hat{\rho}\} + 2\hat{\sigma}_k^+\hat{\sigma}_k^-\hat{\rho}\hat{\sigma}_k^+\hat{\sigma}_k^-) \tag{8}$$

destroys quantum coherence in the network, where γ_k is a site-dependent dephasing rate. In all these, $\{\star,\rho\}$ denotes the anticommutator $\{\star,\rho\} \equiv \star\rho + \rho\star$. It is important to remark that Eq. (8) is not, however, the only source of decoherence or progressive attenuation of nondiagonal elements of the density matrix in the energy basis. Actually, the pump (6) and the drain (7) are also nonunitary elements, which pushes the system to a diagonal density matrix. In this sense, they also cause decoherence or dephasing, but at the same time they change the network energy.

Our main goal is to study the contribution of each of these terms in the master equation to the dynamics of energy propagation in the QN depicted in Fig. 1. Moreover, we want to investigate it taking into account the presence of initial quantum correlations in the control sites 2 and 4. An important figure of merit is how efficiently energy leaves the system through site 3, which works as a drain (rate Γ_d). This is quantified by the integrated population of site 3,

$$P_3 = \int_0^t p_{33}(t')dt', \tag{9}$$

where $p_{33}(t)$ is the occupation of site 3 at instant $t > 0$. The physical motivation behind this choice can be appreciated by saying that energy leaking site 3 at rate Γ_d is going into a sink (another two-level system) [4]. Although the equation of motion changes a little, by using a sink it can be explicitly shown that P_3 is a good quantifier of transport efficiency. This is so because the sink population at time t turns out to be proportional to P_3 as defined in Eq. (9). In our case, this quantity is not necessarily bounded by one because the network is subjected to continuous energy pump through Eq. (6) and there are no other energy leakages besides transfer to the sink. In some previous studies [9,20], this quantity is bounded since the initial network state usually has one excitation and there is no energy pump. In addition to that, there are also recombination mechanisms that spoil the transport causing energy other leakages. We do not include these recombinations here since our study is not dedicated to molecular energy transfers but to controlled coupled systems with just a few elements such as trapped ions or superconducting qubits. In these settings, there is no sense in talking about typical many-body effects such as exciton recombination or trapping. As a final remark, in the kind of study presented in [9,20], the integral in Eq. (9) is typically evaluated with $t \to \infty$ because one is considering the final stationary state where all quantum correlations have been washed out. Here we are more interested in the first moments of transport precisely in order to check the influence of originally present quantum correlations.

One might also be interested in looking into how energy available at site 3 compares to the network energy. The latter consists of the energy pumping in (out) the system through site 1 (3) as well as energy initially available in the network due to its initial state. Mathematically, we evaluate R_E defined as

$$R_E = \frac{\langle E_3(\tau)\rangle}{\langle\hat{\mathcal{H}}(t)\rangle} = \frac{E_3(t)p_{33}(t)}{\text{Tr}[\rho(t)\hat{\mathcal{H}}(t)]}, \tag{10}$$

i.e., the ration between the average energy of site 3 (coupled to the sink) and the average energy in the network, both at time t.

Finally, in this work we use the entanglement of formation (EoF) to quantify bipartite entanglement between pairs of sites [21]. In addition to that, we also include another form of quantum correlation in our study, the so-called quantum discord (QD) [22]. The latter is interesting because it spots quantumness for a set of states that does not necessarily contain entanglement. In this sense, the QD adds generality to our study.

III. RESULTS

The just presented formalism allows one to explore site-dependent dephasing scenarios. However, from now on we will be adopting the same decoherence rates for all sites $\gamma_k = \gamma$, a feasible choice for quantum technologies. However, if one aims at studying transport in natural systems such as photosynthetic complexes, site-dependent dephasings should necessarily be taken into account in accord with experimental observations and computational simulations.

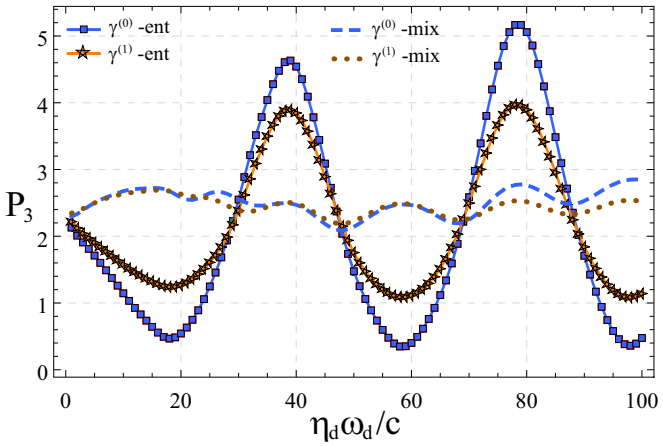

FIG. 2. Integrated population of site 3 [Eq. (9)] as a function of the rescaled driving strength $\eta_d\omega_d/c$ for the parameters $\omega_j = \omega_0 \forall\, j$; $\Delta\omega = \omega_0/4$; $\phi_x = \pi$; $\phi_y = \pi$; $\Theta_1 = 1$; $\Theta_2 = 0$ (energy ladder along the x direction); $c_{j,k} = c = \omega_0/100 \forall j,k$; $\omega_d = \omega_0/4$; $\gamma_k = \gamma \forall k$; $\gamma^{(0)} = \gamma = 0$; $\gamma^{(1)} = \gamma = c/10$; $\Gamma_d = c/100$; and $\Gamma_s = 2\,\Gamma_d$. Here -ent is the initial state in Eq. (11) and -mix is the initial state in Eq. (12).

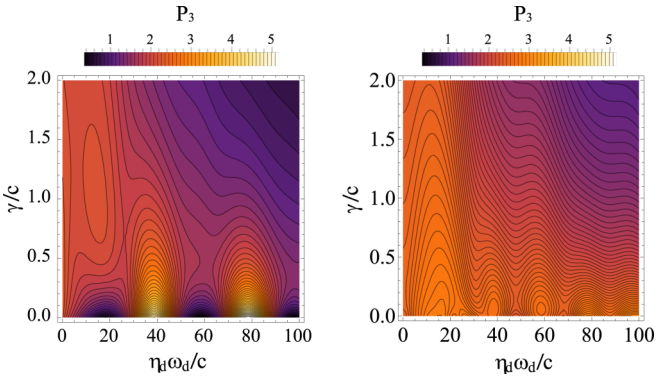

FIG. 3. Efficiency indicator P_3 as a function of the rescaled driving strength $\eta_d\omega_d/c$ and the dephasing γ/c considering the initial state (11) (left) and the initial state Eq. (12) (right). The parameters are the same as in Fig. 2.

A. Efficiency enhancers: Entanglement versus dephasing

We would like to start our investigation by considering two initial states, with the same mean energy (one excitation) but with different types of correlations. The first state is

$$\rho_{\text{ent}} = |\psi\rangle\langle\psi|, \tag{11}$$

where $|\psi\rangle = (|gegg\rangle + |ggge\rangle)/\sqrt{2}$. For this initial preparation, sites 1 and 3 start in their ground state and they are not correlated with sites 2 and 4, which share a bipartite maximally entangled state that contains one quantum of excitation. Experimentally, bipartite entangled states such as the one considered here have been generated in a variety of setups ranging from photons [23] to massive particles [24]. In the scenario defined by Eq. (11), sites 2 and 4 are then quantum correlated. The second initial state to be considered in this section is

$$\rho_{\text{mix}} = (|gegg\rangle\langle gegg| + |ggge\rangle\langle ggge|)/2, \tag{12}$$

where once again sites 1 and 3 are initially in their ground state but now sites 2 and 4 are just classically correlated in a maximally mixed state. One can consider Eq. (12) as the limit of Eq. (11) when previous decoherence ($t < 0$) on the decoupled model ($c = 0$) had fully acted and completely destroyed the coherences, i.e., the nondiagonal terms in the basis $\{|gegg\rangle, |ggge\rangle\}$.

In Fig. 2 we present the efficiency quantifier (9) for an observation time $ct = 10$ (interval of integration) and a dephasing rate $\gamma = c/10$, which means that the dephasing times are around one order of magnitude longer than the hopping times (coherent dynamics). Within this time interval, which can be called a short interaction time, quantum effects have a chance to manifest or to have some influence on transport. In the long-time regime, to be briefly discussed next, quantum effects usually become irrelevant since dephasing generally eliminates the coherences.

In this scenario, by comparing the plots in Fig. 2, it is clear that the initial presence of entanglement helped transport, i.e., resulted in values of P_3 that surpassed those obtained with the initially mixed (nonentangled) situation. In other words, entanglement worked as a resource for QT. Another interesting feature of Fig. 2 is the presence of NAT for the minima when entanglement was originally present at sites 2 and 4. By increasing the dephasing, the efficiency increased in those regions. This is not true for the maxima where dephasing tends to be destructive. This is expected because dephasing destroys entanglement in our model and entanglement is precisely the ingredient for the pronounced maxima. For the initial mixed state, the phenomenon of NAT is practically absent in Fig. 2. Although the presence of entanglement is the ingredient that provides the global maximum in Fig. 2, it is necessary to point out that there are values of amplitude for which the mixed state preparation leads to better efficiency.

All these interesting features are confirmed by Fig. 3, where we provide a more general picture of the problem through variation of dephasing over a broad range. It is interesting to see that for the initial preparation with entanglement (plot on the left), increasing the dephasing γ is generally beneficial for the minima and that this feature is practically not manifested for the nonentangled initial situation (plot on the right). On the contrary, dephasing acted as a hinderer when no entanglement was initially present.

We now present the long-time behavior of the population p_{33} of the last site, fixing two values of $\eta_d\omega_d/c$: the first minimum and the first maximum of P_3 with initial entanglement in Fig. 2. The results are shown in Fig. 4, where one can see that initial entanglement, as expected, gradually loses its capacity to boost transport. The only enhancer left is dephasing through NAT. This mechanism is clearly manifest in Fig. 4, given the fact that, for times longer than $ct \approx 60$, the curves with non-null dephasing $\gamma^{(1)}$ are above the ones with null dephasing $\gamma^{(0)}$.

Before finishing this section, we would like to go a little deeper in our investigation about the entanglement-assisted transport phenomenon already observed in previous plots. We will do this in three directions. First, we would like to see how Fig. 2 changes when the input of energy is changed. This is shown in Fig. 5. The plots are very illustrative because they once again show the competition between entanglement-

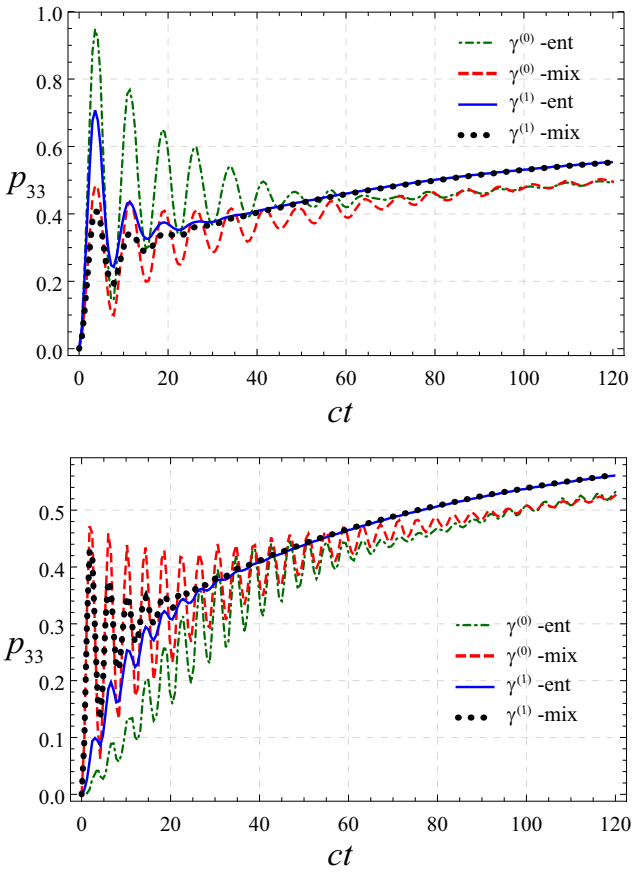

FIG. 4. Temporal dependence of the population of site 3, p_{33}, for the first minimum ($\eta_d\omega_d/c = 18.0$) and maximum ($\eta_d\omega_d/c = 38.8$) values in Fig. 2. Here -ent is the initial state in Eq. (11) and -mix is the initial state in Eq. (12). Shown on top is the first maximum and on bottom the first minimum. The other parameters are the same as in Fig. 2.

assisted transport and noise-assisted transport, now for a different scenario where the increase of noise comes from sources other than pure dephasing. For $\Gamma^{(1)}$, the beneficial effect coming from initial entanglement is still quite clear, almost like in Fig. 2. To see this, compare, for instance, the maxima arising from the situation with initial maximal entanglement with that of maximal mixedness. When the incoherent input of energy is increased to $\Gamma^{(2)}$, the initial maximally mixed state and the initial maximally entangled state are practically equivalent in terms of efficiency. The reason why initial entanglement starts losing importance when the energy input rate increases is that adding more energy also adds more noise. This is so because the energy input and output are both incoherent process corresponding to nonunitary terms in the network master equation [see Eqs. (6) and (7)].

The second direction we want to explore is the variation of the initial entanglement. Up to now, we worked only with maximal entanglement versus nonentanglement, both states with only one excitation shared between sites 2 and 4. We now consider the one excitation sector, but with the state $|\psi\rangle = \cos\theta|eg\rangle + \sin\theta|ge\rangle$ for sites 2 and 4. The other two sites are still considered to be initially in the ground state. The variation of θ makes the entanglement of formation vary from zero

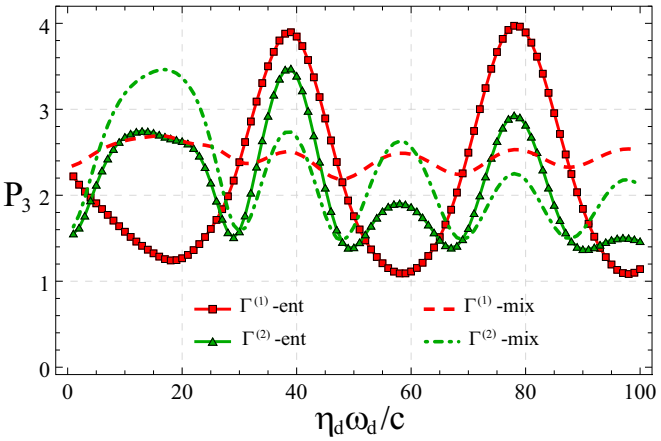

FIG. 5. Integrated population of site 3, for the two drain rates $\Gamma^{(1)} = c/100$ and $\Gamma^{(2)} = c/10$. The chosen dephasing rate is $\gamma = c/10$. Here -ent is the initial state in Eq. (11) and -mix is the initial state in Eq. (12). The other parameters are the same as in Fig. 2.

($\theta = 0$) to one ($\theta = \pi/4$). In Fig. 6 we once again consider the efficiency indicator P_3 in the first maximum $\eta_d\omega_d/c = 38.8$ (see Fig. 2). However, we now have it as a function of dephasing and the entanglement in the initial state $|\psi\rangle$. One can see that states with more initial entanglement lead to higher values of P_3. This confirms the robustness of the entanglement-assisted transport mechanism for a whole class of states (all pure states with one excitation shared by control sites 2 and 4). Finally, one can see once again that, for initial pure states and the maxima of P_3 in Fig. 2, the increase of dephasing γ is a hindrance to transport.

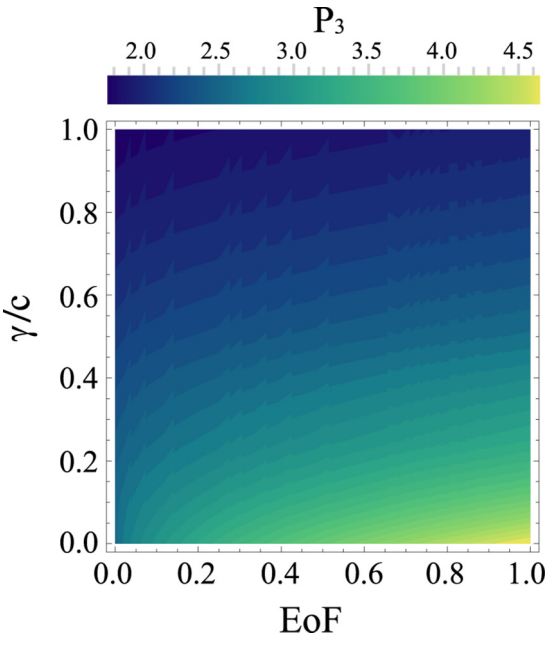

FIG. 6. Efficiency indicator P_3, as a function of dephasing and entanglement in the initial state, for the first maximum ($\eta_d\omega_d/c = 38.8$) in Fig. 2. The drain rate is $\Gamma_d = c/100$. The other parameters are the same as in Fig. 2.

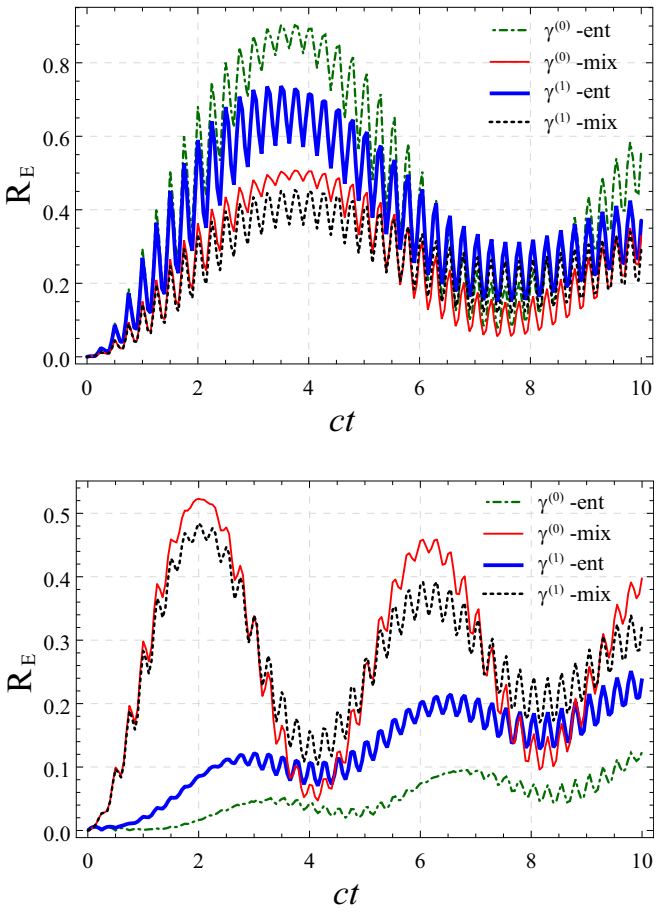

FIG. 7. Temporal dependence of R_E defined in Eq. (10) for the first maximum in Fig. 2 ($\eta_d\omega_d/c = 38.8$) (top) and the first minimum ($\eta_d\omega_d/c = 18.0$) (bottom). Here -ent is the initial state in Eq. (11) and -mix is the initial state in Eq. (12). The other parameters are the same as in Fig. 2.

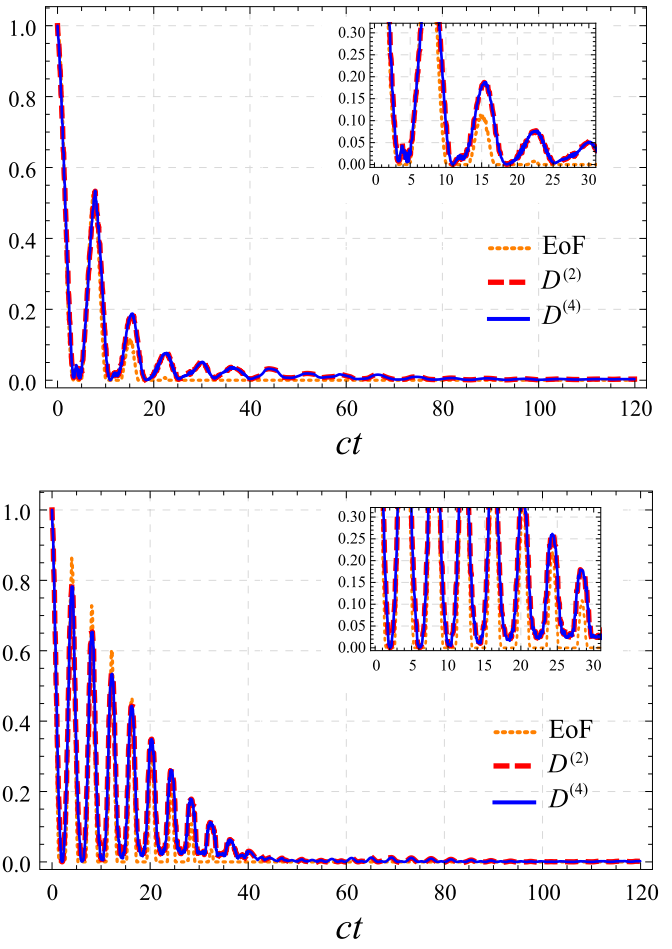

FIG. 8. Temporal dependence of the QC between sites 2 and 4 for the first maximum (top) and the first minimum (bottom). The insets show close-ups intended to highlight the existence of QC apart from entanglement for several times. The initial state is Eq. (11). Here $\gamma_k = 0\forall k$ and $\Gamma_d = c/100$. The other parameters are the same as in Fig. 2.

The third and final direction has to do with the energy being transported to site 3. Clearly, the result of this analysis must agree with the findings based on the use of Eq. (9). In Fig. 7 we present the dynamics of R_E as defined in Eq. (10). It is clear that for the first maximum in Fig. 2, which is considered for the top plot in Fig. 7, the presence of entanglement is indeed more advantageous for the transport. The bottom plot in Fig. 7 also confirms that, for the first minimum in Fig. 2, it is the mixed state that provides the best choice. However, the global maximum of R_E in Fig. 7 is a consequence of the initial entanglement as pointed out before.

B. Quantum correlation survival

Since the initial presence of entanglement was seen to be beneficial for transport in the short-time behavior, it would be interesting to have a close look at its dynamics. This could help us to better understand the conclusions previously presented about the effect of quantum correlations (QCs) over transport for our system of interest. As said before, we will be employing quantifiers of entanglement and quantum discord QD. For the latter, it is important to distinguish between the situation where projective measurements are thought to act on one subsystem or another. In our case, the subsystems are sites 2 and 4 and we will then denote the cases where projective measurements are intended to act on 2 by $D^{(2)}$ and on 4 by $D^{(4)}$. The dynamical behaviors of entanglement and discord are shown in Fig. 8. As expected, at long times the oscillatory behavior of the quantum correlations is completely damped, rendering the system state to be essentially classicality correlated. It is interesting to see that there are times where quantum discord remains finite in spite of the fact that entanglement goes to zero. In Fig. 9 we present the average correlations over the same time span considered to evaluate P_3 in Fig. 2, for an initially maximally entangled situation. From this plot it is clear that also on average quantum correlations remain finite during the transport for the whole range of driving strengths $\eta_d\omega_d/c$ considered in Fig. 2. From Fig. 9 it is also possible to see that entanglement is a bit more sensitive to the choice of the driving strength than discord in the sense that the former oscillates more strongly than the latter as the driving strength is varied.

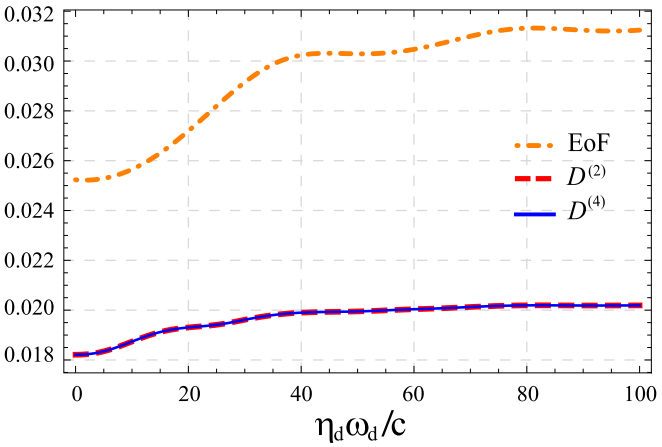

FIG. 9. Temporal average of QC between sites 2 and 4 for the situation where the system is initially in an entangled state. A large dephasing situation is considered, with $\gamma_k = c\forall k$ and $\Gamma_d = c/100$, for the initial state (11). The other parameters are the same as in Fig. 2.

IV. CONCLUSION

In this work we studied the relation between transport efficiency and initial presence of entanglement in a network. The network used in this work is the simplest one needed to assess the effect of having entanglement in the intermediate sites, i.e., between two sites not directly connected to energy sources or sinks. In fact, we found that initial entanglement provides a robust enhancer of transport efficiency. For short times, entanglement-assisted transport showed up for all possible initial pure states with only one excitation in the network. In this time domain, we showed that quantum correlations survive dynamically and on average thus rendering the transport to be quantum in essence. On the other hand, for longer times, these correlations progressively vanish and it reaches a point where only noise-assisted transport is available as a transport enhancer. We also showed that, for short times, noise-assisted transport is immaterial for the maximally mixed initial situation.

As a final remark, for the systems one has in mind when talking about quantum technologies (trapped ions, etc.), the decoherence model employed here successfully describes the general observed features of the open system dynamics. However, if one thinks of considering energy transport in molecular systems or condensed matter systems, the strong coupling to the environment degrees of freedom typically invalidates the first-order master equation in the Born and Markov approximations as employed here. In this case, more sophisticated treatments such as mappings onto a one-dimensional system allowing the use of the time-adaptive density matrix renormalization group techniques are necessary to deal with the time evolution of the full system [25].

ACKNOWLEDGMENTS

A.A.C. acknowledges Coordenação de Aperfeiçoamento de Pessoal de Nível Superior. F.L.S. acknowledges partial support from the Brazilian National Institute of Science and Technology of Quantum Information and CNPq under Grant No. 307774/2014-7. We would also to thank Marcela Herrera and Professor Roberto Serra for granting access to their computing facilities.

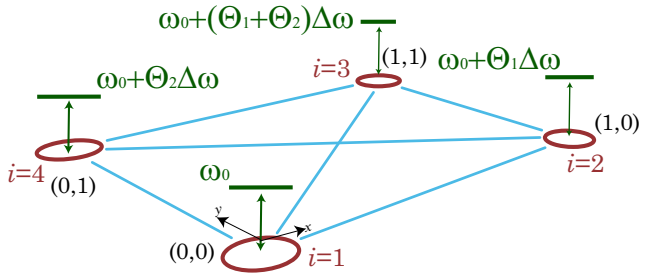

FIG. 10. Network and its basic elements. Four two-level systems labeled by i occupy the sites at $\mathbf{i} = (i_1,i_2)$ forming the network. The lines connecting the sites represent their coherent interaction (3) with coupling strength c_{jk}. The site-dependent energies are also indicated.

APPENDIX A: EFFECTIVE HAMILTONIAN

In this appendix we provide details about the external drivings that are responsible for the effective suppressing of possible couplings between sites 1 and 3 and between sites 2 and 4. In Fig. 10 we present the four-site network with arbitrary coupling constants c_{jk} between sites j and k. The form of the interaction is that giving by the Hamiltonian (3). We say that site i $(i = 1,2,\ldots)$ is located at $\mathbf{i} = (i_1,i_2)$, where i_1 and i_2 are natural numbers (zero included). Also, the external drive phases are chosen to be site dependent

$$\phi_i = i_1\phi_x + i_2\phi_y. \tag{A1}$$

All these driving parameters and the energy ladder $\Delta\omega_j$ are controlled externally and provide a variable tool to design effective interactions in the network [15,16].

For the sake of simplicity, we will now choose the driving field controlled parameters such that $\omega_{d,j} = \omega_d$ and $\eta_{d,j} = \eta_d$, for each site j. Also, we consider $\omega_j = \omega_0$ and $\Delta\omega = r\omega_d$, with r a positive integer, which forms an energy ladder implemented via the time-independent part of the external field (see Fig. 10). From Eq. (4) it follows that $\Delta\omega_1 = 0$, $\Delta\omega_2 = \Theta_1\Delta\omega$, $\Delta\omega_3 = (\Theta_1 + \Theta_2)\Delta\omega$, and $\Delta\omega_4 = \Theta_2\Delta\omega$. Also, by using Eq. (A1), one finds that

$$\begin{aligned}\phi_1 &= 0,\\ \phi_2 &= \phi_x,\\ \phi_3 &= \phi_x + \phi_y,\\ \phi_4 &= \phi_y.\end{aligned} \tag{A2}$$

The hopping Hamiltonian (3) naturally appears in various scenarios. It may represent, for instance, dipole-dipole interaction among two-level atoms or molecules in free space [26]. Another well-known situation where the Hamiltonian (3) appears is the dispersive interaction of two-level systems with a common bosonic mode [27]. The role of the driving is to suppress the coupling between particular pairs of sites. Our goal is to carefully choose the phases of the external driving fields to design an effective regime where the transitions between sites 1 and 3 and between sites 2 and 4 are suppressed.

With this, we can study how energy injected at site 1 arrives at site 3 through indirect pathways $1 \leftrightarrow 2 \leftrightarrow 3$ and $1 \leftrightarrow 4 \leftrightarrow 3$, as depicted in Fig. 1. This is a situation found, for instance, in the description of the conduction of potassium ions in the KcsA channel [28–30]. This suppression is achieved as follows.

By transforming the system Hamiltonian (1) to an interaction picture with respect to $\hat{\mathcal{H}}_0$ and taking into account the condition $\Delta\omega = r\omega_d$ (r a positive integer), a rotating-wave approximation (RWA) can be performed to obtain

$$\hat{\mathcal{H}}_I = \hbar \sum_{ij;k>j} \tau_{jk}(\hat{\sigma}_j^+ \hat{\sigma}_k^- + \hat{\sigma}_j^- \hat{\sigma}_k^+), \tag{A3}$$

with

$$\tau_{jk} \equiv c_{jk}\mathcal{F}_{f(r,j,k)}(\eta_d, \Delta\phi_{j,k}) e^{-i[f(r,j,k)/2](\phi_j+\phi_k)}, \tag{A4}$$

where

$$f(r,j,k) \equiv r[(\Theta_1 j_1 + \Theta_2 j_2) - (\Theta_1 k_1 + \Theta_2 k_2)], \tag{A5}$$

$$\Delta\phi_{j,k} \equiv \phi_j - \phi_k, \tag{A6}$$

and

$$\mathcal{F}_\chi(\xi,\zeta,\theta) \equiv \sum_{s=-\infty}^{\infty} \mathcal{J}_s(\xi)\mathcal{J}_{s+\chi}(\zeta) e^{i(s+\chi/2)\theta}, \tag{A7}$$

with $\mathcal{J}_s$ being the Bessel function of first kind and order s [31,32]. The rotating-wave approximation used to obtain (A3) is valid only for $c_{j,k} \ll \omega_0, \omega_d$ [14]. In other words, the coupling constants must be weaker than the natural frequencies of the on-site transitions. This is the common scenario found in the majority of the controlled systems such as trapped ions or cavity quantum electrodynamics. As a matter of fact, strong couplings between the subsystems that surpass the natural transition frequencies are very hard to implement in general. It is actually a current line of investigation in circuit quantum electrodynamics called an ultrastrong-coupling regime [33]. Only in such rare conditions would the hierarchy of parameters used here not be observed.

Now we carefully look into the content of Eq. (A3). For the sake of simplicity, let us consider once again $r = 1$. The dynamics of energy migration between sites i and j is ruled by $\mathcal{F}_{f(1,j,k)}$ [see Eq. (A4)]. The magnitude of this quantity for the pair of diagonal sites 1 and 3 and sites 2 and 4 is plotted in Fig. 11 as a function of the driving parameters. Direct inspection Fig. 11 and Eqs. (A2) and (A6) thus reveals that the choice $\phi_x = \phi_y = \pi$ leads to the sought suppression of hopping along those diagonal sites. This is true regardless of the driving amplitude η_d for the range of parameters considered. It is this choice of ϕ_x and ϕ_y together with the full original (non-RWA) time-dependent Hamiltonian (1) that has been used in the simulations. The RWA argument was just used to understand how the external driving can effectively suppress hopping between particular pair of sites.

APPENDIX B: IMPORTANCE OF THE SITE-DEPENDENT PHASES

We now consider the relevance of the site-dependent phases in Eq. (2). As we are going to show, it goes well beyond the construction of the topology sketched in Fig. 1. For that, let

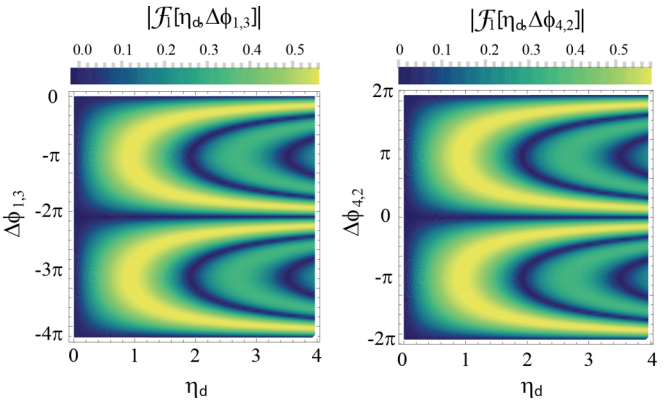

FIG. 11. Effective hopping amplitude between sites j and k [Eq. (A7)] as a function of the driving amplitude η_d and phase $\Delta\phi_{jk}$. In particular, $|\mathcal{F}_1| \equiv |\mathcal{F}_{f(1,j,k)}|$is considered, where $r = 1$. Shown on the left are sites 1 and 3 and on the right sites 2 and 4. The parameters used are $\Theta_1 = 1$ and $\Theta_2 = 0$.

us suppose the following Hamiltonian where all such phases have been dropped:

$$\hat{\mathcal{H}}'(t) = \sum_j E'_j(t)\hat{\sigma}_j^+\hat{\sigma}_j^- + \sum_{k>j} c(\hat{\sigma}_j^+\hat{\sigma}_k^- + \hat{\sigma}_j^-\hat{\sigma}_k^+). \tag{B1}$$

Here

$$E'_j(t) = \omega_j + \Delta\omega_j(\Theta_1 j_1 + \Theta_2 j_2) + \lambda\eta_{d,j}\omega_{d,j}\cos(\omega_d t) \tag{B2}$$

and λ is an auxiliary parameter assuming the value zero or one. The choice $\lambda = 0$ leave us with a time-independent Hamiltonian, from which no dependence on $\eta_{d,j}$ can appear. Consequently, most of our findings cannot be obtained within this approach, for example, Figs. 2, 3, and 5. For $\lambda = 1$, i.e., a time-dependent Hamiltonian with no site-dependent phases, and $\eta_{d,j} = \eta_d$ for all j, we obtain the plots in Fig. 12. It is clear once again that no dependence on η_d appears, just like in the case $\lambda = 0$. This independence from η_d is actually quite intriguing. In order to spot its origin, we once again move to the interaction picture, turning the Hamiltonian in Eq. (B1)

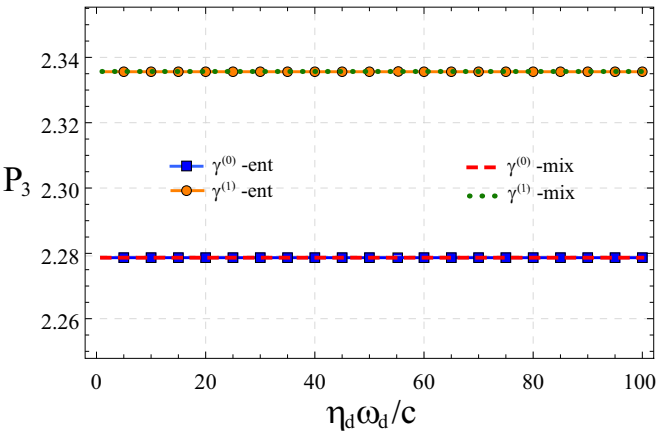

FIG. 12. Integrated population of site 3 as a function of rescaled driving strength $\eta_d\omega_d/c$. The parameters are the same as in Fig. 2.

into

$$\hat{\mathcal{H}}_I = \sum_{k>j} \{\varrho_{j,k}\hat{\sigma}_j^+\hat{\sigma}_k^- + \text{H.c.}\}, \tag{B3}$$

where $\varrho_{j,k} \equiv c\,\mathcal{G}_{f(r,j,k)}(\eta_{d,j},\eta_{d,k})$ and $\mathcal{G}_\chi(\xi,\zeta) \equiv \sum_{s=-\infty}^{\infty}\mathcal{J}_s(\xi)\mathcal{J}_{s+\chi}(\zeta)$. Like before, we set $\Theta_1 = 1$, $\Theta_2 = 0$, $\eta_{d,j} = \eta_{d,k} = \eta_d$, and $r = 1$. By using the Neumann addition theorem for Bessel functions [34], one can show that

$$\sum_{s=-\infty}^{\infty}\mathcal{J}_s(\eta_d)\mathcal{J}_{s+f(1,j,k)}(\eta_d) = \mathcal{J}_{f(1,j,k)}(0). \tag{B4}$$

Consequently, $\mathcal{G}_{f(1,j,k)}(\eta_d) = \mathcal{J}_{f(1,j,k)}(0)$, which is completely independent from η_d. From all these considerations, it is clear that the site-dependent phases play a fundamental role in all facets of this transport problem.

[1] H. Rabitz, Focus on quantum control, New J. Phys. **11**, 105030 (2009).

[2] M. Mohseni, Y. Omar, G. Engel, and M. B. Plenio, *Quantum Effects in Biology* (Cambridge University Press, Cambridge, 2014).

[3] M. B. Plenio and S. F. Huelga, Dephasing-assisted transport: Quantum networks and biomolecules, New J. Phys. **10**, 113019 (2008).

[4] F. Caruso, A. W. Chin, A. Datta, S. F. Huelga, and M. B. Plenio, Highly efficient energy excitation transfer in light-harvesting complexes: The fundamental role of noise-assisted transport, J. Chem. Phys. **131**, 105106 (2009).

[5] A. W. Chin, A. Datta, F. Caruso, S. F. Huelga, and M. B. Plenio, Noise-assisted energy transfer in quantum networks and light-harvesting complexes, New J. Phys. **12**, 065002 (2010).

[6] A. W. Chin, S. F. Huelga, and M. B. Plenio, Coherence and decoherence in biological systems: Principles of noise-assisted transport and the origin of long-lived coherences, Philos. Trans. R. Soc. A **370**, 3638 (2012).

[7] B.-q. Ai and S.-L. Zhu, Complex quantum network model of energy transfer in photosynthetic complexes, Phys. Rev. E **86**, 061917 (2012).

[8] F. L. Semião, K. Furuya, and G. J. Milburn, Vibration-enhanced quantum transport, New J. Phys. **12**, 083033 (2010).

[9] M. Mohseni, P. Rebentrost, S. Lloyd, and A. Aspuru-Guzik, Environment-assisted quantum walks in photosynthetic energy transfer, J. Chem. Phys. **129**, 174106 (2008).

[10] F. Caruso, A. W. Chin, A. Datta, S. F. Huelga, and M. B. Plenio, Entanglement and entangling power of the dynamics in light-harvesting complexes, Phys. Rev. A **81**, 062346 (2010).

[11] M. Sarovar, A. Ishizaki, G. R. Fleming, and K. B. Whaley, Quantum entanglement in photosynthetic light-harvesting complexes, Nat. Phys. **6**, 462 (2010).

[12] K. Bradler, M. M. Wilde, S. Vinjanampathy, and D. B. Uskov, Identifying the quantum correlations in light-harvesting complexes, Phys. Rev. A **82**, 062310 (2010).

[13] F. Nicacio and F. L. Semiao, Transport of correlations in a harmonic chain, Phys. Rev. A **94**, 012327 (2016).

[14] F. Nicacio and F. L. Semiao, Coupled harmonic systems as quantum buses in thermal environments, J. Phys. A: Math. Theor. **49**, 375303 (2016).

[15] A. Bermudez, T. Schaetz, and D. Porras, Synthetic Gauge Fields for Vibrational Excitations of Trapped Ions, Phys. Rev. Lett. **107**, 150501 (2011).

[16] A. Bermudez, T. Schaetz, and D. Porras, Photon-assisted-tunneling toolbox for quantum simulations in ion traps, New J. Phys. **14**, 053049 (2012).

[17] M. Grifoni and P. Hänggi, Driven quantum tunneling, Phys. Rep. **304**, 229 (1998).

[18] M. Glück, A. R. Kolovskya, and H. C. Korsch, Wannier-Stark resonances in optical and semiconductor superlattices, Phys. Rep. **366**, 103 (2002).

[19] H. J. Carmichael, *Statistical Methods in Quantum Optics 1: Master Equations and Fokker-Planck Equations* (Springer, Berlin, 2002).

[20] P. Rebentrost, M. Mohseni, I. Kassal, S. Lloyd, and A. Aspuru-Guzik, Environment-assisted quantum transport, New J. Phys. **11**, 033003 (2009).

[21] W. K. Wootters, Entanglement of Formation of an Arbitrary State of Two Qubits, Phys. Rev. Lett. **80**, 2245 (1998).

[22] H. Ollivier and W. H. Zurek, Quantum Discord: A Measure of the Quantumness of Correlations, Phys. Rev. Lett. **88**, 017901 (2001).

[23] G. Weihs, T. Jennewein, C. Simon, H. Weinfurter, and A. Zeilinger, Violation of Bell's Inequality under Strict Einstein Locality Conditions, Phys. Rev. Lett. **81**, 5039 (1998).

[24] M. Steffen, M. Ansmann, R. C. Bialczak, N. Katz, E. Lucero, R. McDermott, M. Neeley, E. M. Weig, A. N. Cleland, and J. M. Martinis, Measurement of the entanglement of two superconducting qubits via state tomography, Science **313**, 1423 (2006).

[25] J. Prior, A. W. Chin, S. F. Huelga, and M. B. Plenio, Efficient Simulation of Strong System-Environment Interactions, Phys. Rev. Lett. **105**, 050404 (2010).

[26] Z. Ficek and S. Swain, *Quantum Interference and Coherence: Theory and Experiments* (Springer, New York, 2005).

[27] P. P. Munhoz and F. L. Semião, Multipartite entangled states with two bosonic modes and qubits, Eur. Phys. J. D **59**, 509 (2010).

[28] J. Morais-Cabral, Y. Zhou, and R. MacKinnon, Energetic optimization of ion conduction rate by the K^+ selectivity filter, Nature (London) **414**, 37 (2001).

[29] S. Bernèche and B. Roux, Energetics of ion conduction through the K^+ channel, Nature (London) **414**, 73 (2001).

[30] A. A. Cifuentes and F. L. Semião, Quantum model for a periodically driven selectivity filter in a K^+ ion channel, J. Phys. B **47**, 225503 (2014).

[31] A. Vaziri and M. B. Plenio, Quantum coherence in ion channels: Resonances, transport and verification, New J. Phys. **12**, 085001 (2010).

[32] G. N. Watson, *A Treatise on the Theory of Bessel Functions*, 2nd ed. (Cambridge University Press, Cambridge, 1966).

[33] T. Niemczyk, F. Deppe, H. Huebl, E. P. Menzel, F. Hocke, M. J. Schwarz, J. J. Garcia-Ripoll, D. Zueco, T. Hummer, E. Solano, A. Marx, and R. Gross, Circuit quantum electrodynamics in the ultrastrong-coupling regime, Nat. Phys. **6**, 772 (2010).

[34] NIST Digital Library of Mathematical Functions, Release 1.0.14 of 2016-12-21, edited by F. W. J. Olver, A. B. Olde Daalhuis, D. W. Lozier, B. I. Schneider, R. F. Boisvert, C. W. Clark, B. R. Miller, and B. V. Saunders; see in particular Eq. (10.23.2).